

## CC-PGI: Imaging prompt gammas with Compton cameras

### Dedicated Monte Carlo simulations and image reconstruction algorithms for range verification in particle therapy using Compton cameras

*N. Kohlase, M. Rafecas, Institute of Medical Engineering, Universität zu Lübeck*

#### In Short

- Particle therapy needs range verification method to ensure a correct dose application in the tumor and to better spare healthy tissue surrounding the tumor.
- Compton cameras (CC) are under investigation as range verification method in particle therapy.
- Accurate simulations of CCs based on Monte Carlo methods help to understand the physical processes and detector limitations in particle therapy.
- To ensure a correct range verification with CCs, dedicated iterative image reconstruction algorithms are needed.

Particle therapy is a widely accepted tumor treatment method, because of its well-defined penetration range and its maximum dose transfer at the end of this range. Therefore the tumor is radiated and the surrounding tissue can be spared. Unfortunately this beam range is susceptible to changes of the tissue composition along the beam path or to changes in the patient position between the daily radiation fractions. For this reason range verification methods are mandatory. Range-verification methods estimate range deviations indirectly, making use of the secondary effects derived from the treatment, like prompt gamma-rays (PG). PGs emerge from atomic nuclei few picoseconds after those nuclei were excited by the beam particles. Most PGs leave the patient body and can be detected. By means of tomographic reconstruction algorithms, a three-dimensional image of the PG emission origins can be generated. As this distribution is correlated to the beam extent, possible range deviations can be identified by inspecting the reconstructed images.

To indirectly measure the range of the particle beams during patient irradiation, Compton cameras (CC) can be used, since they provide information about the incoming PGs. In the ideal case, the incoming photon undergoes a Compton interaction in the front detector layers, the so-called *scatterers*; subsequently, the scattered photon is photoelectrically absorbed in another detector layer, the *absorber*. Using the information related to the two interactions, the origin of the photon can be restricted

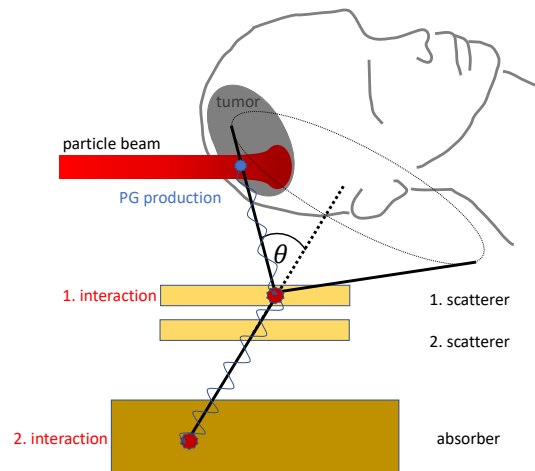


**Figure 1:** Principle of CC imaging. The PG is produced within the particle beam, is Compton scattered in the scatterer and then photoelectric absorbed in the absorber.

to a half-cone, where the first interaction position defines the cone vertex. Using Compton kinematics the cone half-angle  $\theta$ , which complies with the Compton scattering angle, can be calculated as:

$$\cos(\theta) = 1 - m_e c^2 \cdot \frac{E_1}{E_2(E_1 + E_2)}; \quad (0.1)$$

$E_1$  and  $E_2$  are the deposited energies under the assumption that the initial energy was  $E_0 = E_1 + E_2$ . Fig. 1 shows the described principle of CC-PG imaging. An event, or coincidence, includes all interactions that were detected within a certain coincidence time window between the detector layers.

Monte Carlo (MC) simulations play an important role in the design and optimization of detector systems. With the help of MC methods, the whole chain can be described, from particle production and beam irradiation to the detection of secondary radiation by the range-verification detectors. Through this chain we are able to produce data for reconstruction and to validate the designed algorithms. In this project, the *Geant4 Application for Emission Tomography* toolkit (GATE) is used [1]. Very recently an extension for CC, *CCmod*, has been introduced into GATE [2].

To visualise radiation sources, such as the PG distribution originating from the irradiation with a particle beam, tomographic reconstruction is needed. The most commonly used algorithms in CC imaging is the *List Mode Maximum Likelihood Expectation Maximization* (LM-MLEM) algorithm [3]. LM-MLEM is based on the optimization of an objective function,

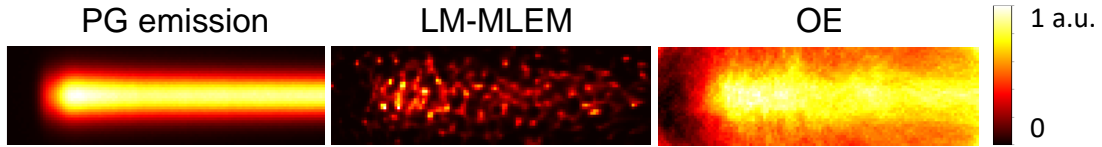


**Figure 2:** Reconstructed images. The first column shows the PG emission, i.e. the output from a Monte Carlo simulation that serve as reference. Column two and three show the images reconstructed with LM-MLEM and OE, respectively.

the Poisson likelihood. For  $M$  events, LM-MLEM provides an iterative refinement of the current image estimate  $f_j^{(n)}$  as:

$$f_j^{(n+1)} = \frac{f_j^{(n)}}{s_j} \sum_{i=1}^M \frac{a_{ij}}{\sum_{j'=1}^N a_{ij'} f_{j'}^{(n)}}. \quad (0.2)$$

Thereby,  $s_j$ , called the sensitivity, corresponds to the detection probability of a photon emitted from voxel  $j$ ;  $a_{ij}$ , called the system matrix, describes the probability that a photon originating from image element  $j$  is detected as the  $i$ -th event.

The *Origin Ensemble* (OE) algorithm has also attracted attention for CC image reconstruction [4]. OE is based on the Metropolis-Hasting algorithm, which is employed to estimate the expected value of the PG emission distribution conditioned on the measured data. The algorithm generates a sequence of samples of the emission distribution (*states*) following a Markov chain. To create the initial state, an emission origin is randomly assigned to each event. Once all events are assigned an origin, for each event  $i$  a new origin is proposed, and this event is relocated at the new origin according to the acceptance probability from state  $X$  to state  $X'$  as

$$A(X \rightarrow X') = \min \left( 1, \frac{a_{ij'} s_j (x_{j'} + 1)}{a_{ij} s_{j'} (x_j)} \right), \quad (0.3)$$

where  $x_j$  is the event density in voxel  $j$  in the current state. The reconstructed image is obtained by averaging over several states, starting after the Markov chain has converged.

Fig. 2 shows the true PG distribution as well as the reconstructed images with LM-MLEM and OE [5]. An issue, clearly visible in Fig. 2, is the very low event statistic. The reconstructed images produced by both algorithms differ: The LM-MLEM image shows a high level of noise, the typical "night sky" artefacts which characterize low-count MLEM reconstruction. In contrast, OE produced blurred images.

Tomographic reconstruction is an ill-posed optimization problem; this means that small changes in the measurement  $y_i$  can lead to great variations in the solution  $f_j$ , especially if the measurements are noisy and affected by errors (as wrongly estimated cone angles). To mitigate these problems, it is necessary to provide additional information about

the unknown image  $f_j$ . This information can be given through so-called *priors*. Simple priors in emission tomography assume that neighbouring voxels have a similar intensity, so that images suffering from night-sky effect are assigned a lower probability as smoother images. The weight put on the prior (degree of belief) is ruled by a parameter. Further parameters might be required.

This project focuses on two objectives. First, the simulation of a realistic MC simulation chain, to evaluate effects on range verification and to draft strategies to deal with degradation effects. And second, implementing priors for both algorithms, to ensure a better image quality and a more precise range verification. By using the HLRN, it becomes possible to run realistic simulations with several settings; this infrastructure also allows us to study in depth the effect on the reconstructed images of the weighting assigned to the priors as well as other parameters. In summary, thanks to the HLRN we can further investigate the capabilities of CCs for PG-based range verification in particle therapy.

## WWW

<https://www.imt.uni-luebeck.de/research/nuclear-imaging.html>

## More Information

- [1] <http://www.opengatecollaboration.org/>
- [2] Ettebest, A, et al, Phys. Med. Biol 65 (2020): 055004, doi: <https://doi.org/10.1088/1361-6560/ab6529>
- [3] Hilaire, E, et al, Phys. Med. Biol 61 (2016): 3127, doi: <https://doi.org/10.1088/0031-9155/61/8/3127>
- [4] Andreyev, A, et al, Med. Phys. 38 (2011): 429, doi: <https://doi.org/10.1118/1.3528170>
- [5] Kohlhase, N, et al, TRPMS 4 (2020): 233, doi: <https://doi.org/10.1109/TRPMS.2019.2937675>

## Funding

DFG Research Grant no. RA 2830/1-1.